AIAA AVIATION Forum
5-9 June 2017, Denver, Colorado
47th AIAA Thermophysics Conference

Evaluation of an Eulerian-Lagrangian Spray Atomization (ELSA) Model for Nozzle Flow: Modeling of Coupling Between Dense and Disperse Regions

Timothy F. Leung* and Clinton P. T. Groth†
University of Toronto Institute for Aerospace Studies
4925 Dufferin Street, Toronto, Ontario, M3H 5T6, Canada

John T. C. Hu‡
Pratt & Whitney Canada
1801 Courtneypark Dr., Mississauga, Ontario, L5T 1J3, Canada

The Eulerian-Lagrangian Spray Atomization (ELSA) model is considered for the prediction of turbulent spray atomization processes associated with liquid fuels. In this approach, the dense spray region is modelled using an Eulerian-based quasi-multiphase model while the disperse spray region is modelled using a Lagrangian droplet model. Unlike other commonly used strictly Lagrangian-based treatments for spray atomization, which rely on comparatively simple empirically-based algebraic models for the liquid sheet breakup to obtain the droplet distribution function (DDF), the Eulerian-based model, albeit still empirical in nature, accounts for the atomizer and initial spray configuration via a possibly more general partial differential equation (PDE) approach. In particular, the dense spray region is considered through the use of two additional scalar transport equations — an equation for the liquid mass fraction and liquid-gas interface area density. In this Eulerian treatment, spray atomization is modelled through the imposition of source terms in the two transport equations which represent the key physical mechanisms such as primary breakup of the liquid sheet, secondary droplet breakup, as well as droplet collision and coalescence. When the spray determined with this treatment is considered to be sufficiently disperse, the DDF is estimated using the liquid mass fraction and liquid-gas interface area density, and is then used as an input to the Lagrangian droplet model. The latter offers advantages for the modelling of drag, droplet collision and coalescence, turbulent dispersion and possible subsequent vaporization and combustion. The primary focus of the present study is the coupling of the Eulerian and Lagrangian approaches. Source terms are introduced to represent the transfer of mass, momentum and liquid mass fraction from the Eulerian to the Lagrangian model. In addition, an input DDF for the Lagrangian approach is estimated based on the liquid volume fraction and interface area density. The model implementation is validated through the comparison of predicted numerical results with other reported experimental results from literature. Numerical results concerning the droplet distribution and Sauter mean diameter (SMD) are presented for the primary breakup of a liquid water jet and a liquid water jet in a crossflow.

I. Introduction

Liquid atomization plays a key role in the mixing between fuel and air in many combustion systems; including those of aerospace propulsion systems.[1] Spray parameters, such as droplet size, spray pattern and evaporation rate, can affect the fuel-air mixture which influences combustion efficiency and pollutant

*Ph.D. candidate, corresponding author, timf.leung@mail.utoronto.ca
†Professor, groth@utias.utoronto.ca
‡Manager, Hot Section Technology, john.hu@pwc.ca

formation.[2] In addition, parameters such as jet penetration and spray angle are valuable to design engineers for facilitating the construction of an effective combustor. Consequently, accurate liquid atomization models are important for the modelling of the combustion process in engines, including gas turbine engines.

In general, a liquid spray can be separated into dense and disperse regions due to differences in the spray structure and breakup mechanisms. In the dense region, the topology of the spray is extremely complex and highly irregular and the concept of a droplet is not well defined in this region. Conversely, in the disperse region, the behaviour of the spray can be rather accurately described by a collection of droplets of varying size and velocity. Due to these inherent differences, different modelling approaches have been developed for the dense and disperse spray regions.[3–5]

In the dense spray region, the spray is commonly modelled by tracking the evolution of the liquid-gas interface which can be either explicitly resolved or modelled. The explicit resolution of the interface movement is difficult as the smallest scale of atomization is not well characterized — there is no analogy to the Kolmogorov length scale in the atomization process. As a consequence, the numerical solution may have some dependence on the grid resolution.[6,7] Additionally, the computational costs associated with the explicit resolution of the liquid-gas interface movement can also be very significant, since the relevant atomization length scales can be on the order of the Kolmogorov scale. At present, these methods generally are only feasible for problems of academic interest where the simulation domain is restricted to be on the order of tens of nozzle diameters.

Alternatively, the evolution of the liquid-gas interface can be modelled using more empirical-based Eulerian methods, such as originally proposed in the Σ-Y model by Vallet *et. al.*[8] The Σ-Y model attempts to characterize the liquid spray with two scalar quantities: the liquid volume fraction, $\bar{Y}$, and the interface area density, $\bar{\Sigma}$. The evolution of the scalar quantities are described using transport equations which contain modelled source terms that describe the atomization processes — the source terms contain dependencies on liquid volume fraction and turbulence quantities. The original model was developed within the framework of the Reynolds Averaged Navier-Stokes (RANS) equations, although efforts have been made to extend the model for Large Eddy Simulations (LES).[9] With the knowledge of $\bar{Y}$ and $\bar{\Sigma}$, it is possible to then determine the Sauter mean diameter (SMD) and droplet number density. In the so-called Eulerian-Lagrangian Spray Atomization (ELSA) model, the SMD and spatial distribution of the droplets arising from the Σ-Y model is used as an input for a secondary Lagrangian spray model, which is initialized in the disperse region of the spray.

In the disperse spray region, the spray is generally assumed to take the form of small, quasi-spherical droplets which can be modelled using a statistical theory based on a droplet distribution function (DDF).[3,10] The evolution of the DDF can be described using the Williams spray equation and the solution is commonly approximated using a Lagrangian treatment by tracking the trajectory of a number of computational parcels, which represent a collection of droplets with identical characteristics (i.e., droplet size, velocity).[3,10] Coupling between the Eulerian gas phase (the gas phase is overwhelmingly treated using an Eulerian approach) and such a Lagrangian treatment for the liquid phase occurs through mass, momentum and energy exchange between phases, where the droplets are considered as point sources and the internal dynamics of the droplets is ignored.[3]

I.A. Scope

In this paper, a comprehensive RANS-based model for describing both the dense and disperse regions of turbulent sprays is developed by coupling the Eulerian Σ-Y model of Lebas *et. al*[11] for describing the dense spray region with a Lagrangian model for the disperse phase. Compared to the empirically-based algebraic models more typically used, the Eulerian Σ-Y model offers a possibly more general PDE-based approach to account for the primary atomization of the spray and initial spray configuration. Transition from the Σ-Y model to the Lagrangian spray model is achieved by using the liquid volume fraction and interface area density to estimate a PDF, which is then used as an initial boundary condition by the Lagrangian spray model. Source terms that describe the transfer of mass and momentum from the Eulerian to the Lagrangian model are proposed to provide an accurate and numerically robust transition. The accuracy of the ELSA, examined herin exclusively for non-reactive spray problems, is assessed through comparison with the experiments performed by Wu *et. al*[12] and Madabhushi *et. al*.[13] In addition, the predicted spray from the ELSA model is compared to predictions made by the Lagrangian discrete phase model (DPM) and the Σ-Y model applied to the entire domain.

II. ELSA Solution Methodology

II.A. Dense Spray Region

The modelling of the dense spray region is considered using the Σ-Y model, as originally developed by Vallet *et. al.*[8] The Σ-Y model is a quasi-multiphase, RANS-based model that treats the fluid as a single mixture and the liquid and gas phases are represented as different species within the mixture. The Reynolds and Weber numbers are assumed to be large so that surface tension and laminar viscosity are negligible. The time-averaged versions of the mass and momentum conservation equations for the mixture are then given respectively by

$$\frac{\partial}{\partial t}\left(\bar{\rho}\right) + \frac{\partial}{\partial x_i}\left(\bar{\rho}\tilde{u}_i\right) = 0\,, \tag{1}$$

$$\frac{\partial}{\partial t}\left(\bar{\rho}\tilde{u}\right) + \frac{\partial}{\partial x_i}\left(\bar{\rho}\tilde{u}_i\tilde{u}_j\right) = -\frac{\partial}{\partial x_i}\left(\bar{P}\right) - \frac{\partial}{\partial x_i}\left(\lambda_{ij}\right)\,, \tag{2}$$

where $\bar{\rho}$, $\tilde{u}_i$ and $\bar{P}$ are the mean mixture density, velocity and pressure, respectively. In the equations above, Reynolds-averaged quantities and the corresponding fluctuations are written as $\bar{\phi}$ and ϕ', while Favre-averaged quantities and the corresponding fluctuations are written as $\tilde{\phi}$ and ϕ''. The Reynolds stress tensor, which arises due to the time averaging process, is given by λ_{ij} and is modelled herin using a variant of the two equation SST k-ω model.[8,11,14] At present, as the focus is on non-reactive spray flows, the effects of heat transfer are neglected so consideration of the energy conservation equation is not required. Modifications have been made to the standard SST k-ω turbulence model to account for pressure diffusion,[11] which can be significant in multiphase flows due to the large density variations. This is described by the following transport equations

$$\frac{\partial}{\partial t}\left(\bar{\rho}\tilde{k}\right) + \frac{\partial}{\partial x_i}\left(\bar{\rho}\tilde{u}_i\tilde{k}\right) = \frac{\partial}{\partial x_i}\left[\left(\frac{\mu_t}{\sigma_k}\right)\frac{\partial\tilde{k}}{\partial x_i}\right] + \lambda_{ij}\frac{\partial\tilde{u}_i}{\partial x_j} - \bar{\rho}\tilde{\epsilon} - \overline{u_i''}\frac{\partial\bar{p}}{\partial x_i}\,, \tag{3}$$

$$\frac{\partial}{\partial t}\left(\bar{\rho}\tilde{\omega}\right) + \frac{\partial}{\partial x_i}\left(\bar{\rho}\tilde{u}_i\tilde{\omega}\right) = \frac{\partial}{\partial x_i}\left[\left(\frac{\mu_t}{\sigma_\omega}\right)\frac{\partial\tilde{\omega}}{\partial x_i}\right] + \alpha\frac{\tilde{\omega}}{\tilde{k}}\left[\lambda_{ij}\frac{\partial\tilde{u}_j}{\partial x_i} - \overline{u_j''}\frac{\partial\bar{p}}{\partial x_j}\right] + \frac{\bar{\rho}\sigma_d}{\tilde{\omega}}\frac{\partial\tilde{k}}{\partial x_j}\frac{\tilde{\omega}}{\partial x_j} - \bar{\rho}\beta\tilde{\omega}^2\,, \tag{4}$$

where the Reynolds average of the Favre fluctuation of the velocity, $\overline{u_i''}$, is related to the turbulent liquid flux, $\bar{\rho}\widetilde{u_i''Y''}$, by

$$\overline{u_i''} = \left(\frac{1}{\rho_l} - \frac{1}{\rho_g}\right)\bar{\rho}\widetilde{u_i''Y''}\,, \tag{5}$$

and where $\tilde{k}$ is the Favre-averaged turbulent kinetic energy, $\tilde{\omega}$ is the Favre-averaged specific turbulent dissipation and μ_t is the turbulent viscosity. Using Equations (3) and (4), together with the Boussinesq approximation, the Reynolds stress tensor can be closed in the following way

$$\lambda_{ij} = \bar{\rho}\widetilde{u_i''u_j''} = \mu_t\left(\frac{\partial\tilde{u}_i}{\partial x_j} + \frac{\partial\tilde{u}_j}{\partial x_i}\right) - \frac{2}{3}\bar{\rho}\tilde{k}\delta_{ij}\,, \tag{6}$$

with

$$\mu_t = \bar{\rho}\frac{\tilde{k}}{\tilde{\omega}}\,. \tag{7}$$

The Σ-Y model introduces two additional scalar transport equations for the liquid volume fraction, $\bar{Y}$, and the interface area density, $\bar{\Sigma}$. However, simplifications to the equations can be made if these scalar quantities are rewritten in terms of unit mass, $\tilde{Y} = \overline{\rho Y}/\bar{\rho}$ and $\tilde{\Omega} = \bar{\rho}\bar{\Sigma}/\bar{\rho}$. The mixture density is obtained by assuming that the liquid and gas phases are incompressible and is given by

$$\frac{1}{\bar{\rho}} = \frac{\tilde{Y}}{\rho_l} + \frac{1-\tilde{Y}}{\rho_g}\,, \tag{8}$$

where ρ_l is the liquid density and ρ_g is the gas density. The transport equation for the liquid mass fraction is then taken to have the form

$$\frac{\partial}{\partial t}\left(\bar{\rho}\tilde{Y}\right) + \frac{\partial}{\partial x_i}\left(\bar{\rho}\tilde{u}_i\tilde{Y}\right) = -\frac{\partial}{\partial x_i}\left(\bar{\rho}\widetilde{u_i''Y''}\right)\,, \tag{9}$$

where the term on the RHS is the turbulent liquid flux. The turbulent liquid flux can be expressed as the difference between the mean liquid and gas velocity (slip velocity) by

$$\widetilde{\bar{\rho} u_i'' Y''} = \bar{\rho}\tilde{Y}(1-\tilde{Y})[\tilde{u}_{l,i} - \tilde{u}_{g,i}]\,, \tag{10}$$

where $\tilde{u}_{l,i}$ and $\tilde{u}_{g,i}$ are the mean liquid and gas velocity, respectively. From this relation, the quasi-multiphase model can be seen as equivalent to the full-multiphase model which explicitly expresses the velocity of each phase. However, the value of the turbulent liquid flux is unknown and an appropriate closure must be specified. A gradient-based closure that makes use of an analogy to Fick's law for molecular diffusion is commonly used, which takes the form

$$\widetilde{\bar{\rho} u_i'' Y''} \approx -\frac{\mu_t}{Sc_t}\frac{\partial \tilde{Y}}{\partial x_i}\,, \tag{11}$$

where μ_t is the turbulent viscosity and Sc_t is the turbulent Schmidt number.

The modelled transport equation for the interface area density, as proposed by Lebas *et. al*,[11] is then given by

$$\frac{\partial}{\partial t}\left(\bar{\rho}\tilde{\Omega}\right) + \frac{\partial}{\partial x_i}\left(\bar{\rho}\tilde{u}_i\tilde{\Omega}\right) = \frac{\partial}{\partial x_i}\left[\left(\frac{\mu_t}{Sc_t}\right)\frac{\partial \tilde{\Omega}}{\partial x_i}\right] + \Psi(S_{init} + S_{turb}) + (1-\Psi)(S_{coll} + S_{2ndBU})\,, \tag{12}$$

$$\Psi(\bar{Y}) = \begin{cases} 1 & \bar{Y} > \bar{Y}_{dense}\,, \\ (\bar{Y} - \bar{Y}_{disperse})/(\bar{Y}_{dense} - \bar{Y}_{disperse}) & \bar{Y}_{disperse} < \bar{Y} < \bar{Y}_{dense}\,, \\ 0 & \bar{Y} < \bar{Y}_{disperse}\,, \end{cases} \tag{13}$$

where $\Psi(\bar{Y})$ is a repartition function that indicates which atomization mechanisms are dominant depending on the dense or disperse region of the turbulent spray. The last four terms on the RHS are source terms which describe the different atomization processes: initialization, primary breakup, collision and coalescence and secondary breakup, respectively.

The $\tilde{\Omega}$ transport equation requires artificial initialization of the $\tilde{\Omega}$ quantity at the injector lips. In the model by Lebas *et al.*,[11] a source term, S_{init}, is proposed to handle the initialization. This term is only significant near the injector and becomes negligible relative to the other source terms after the initial interface area density is created. The initialization term is defined as

$$S_{init} = \alpha_1 \frac{12\bar{\rho}\mu_t}{\rho_l \rho_g Sc_t l_t}\frac{\partial \tilde{Y}}{\partial x_i}\frac{\partial \tilde{Y}}{\partial x_i}, \qquad Sc_t = 0.9\,, \tag{14}$$

where l_t is the turbulent length scale.

Following the approach by Lebas *et al.*,[11] the remaining interface area source terms are defined based on relaxation processes with corresponding characteristic time scales and equilibrium interface area densities. The equilibrium values of $\tilde{\Omega}$ are determined by the definition of an equilibrium Weber number based on the relevant processes. In the dense region of the spray, it is assumed that liquid turbulence is the dominant breakup mechanism. The turbulent source term, S_{turb}, represents the production/destruction of the interface area density due to turbulent flow stretching and collision and coalescence of the jet ligaments — this process is driven by a turbulent time scale, τ_t, which is calculated using the standard k-ω turbulence model definition. The turbulent source term is assumed to proceed towards an equilibrium state, defined by $\tilde{\Omega}^*_{turb}$. It is assumed that the equilibrium state will be reached when the ratio of kinetic energy to surface energy of the jet ligaments is constant. At present, the equilibrium ratio is assumed to take a value of unity, although this may be modified in the future. From the equilibrium ratio, $\tilde{\Omega}^*_{turb}$ may be calculated. The turbulent source term, turbulent time scale and equilibrium turbulent interface area density terms are defined as, respectively,

$$S_{turb} = \alpha_2 \frac{\bar{\rho}\tilde{\Omega}}{\tau_t}\left(1 - \frac{\tilde{\Omega}}{\tilde{\Omega}^*_{turb}}\right), \qquad \tau_t = \frac{\tilde{k}}{\beta^*\tilde{\omega}}, \qquad \tilde{\Omega}^*_{turb} = \frac{\bar{Y}\tilde{k}}{\sigma_l We^*_{turb}}, \qquad We^*_{turb} = 1\,. \tag{15}$$

In the disperse region of the spray, it is assumed that the relevant processes are: droplet collision, droplet coalescence and secondary breakup. The effects of collision and coalescence are represented by the source term S_{coll}. The collision time scale, $\tau_{coll} = l^3_{mean}/S_{eff}\Delta v$, is calculated based on the droplet mean free path,

l_{mean}, collision cross-section, S_{eff}, and the relative velocity between droplets, Δv. The relative velocity can be estimated using the turbulent kinetic energy. The equilibrium state, $\tilde{\Omega}^*_{coll}$, is calculated based on an equilibrium diameter, D_{crit}. Similar to Vallet *et al.*,[8] the equilibrium diameter is calculated using an energy balance, however, this new definition allows the droplets to retain kinetic energy after breakup,[15].[11] The collision breakup and coalescence model can be summarized as follows:

$$S_{coll} = \alpha_3 \frac{\bar{\rho}\tilde{\Omega}}{\tau_{coll}} \left(1 - \frac{\tilde{\Omega}}{\tilde{\Omega}^*_{coll}}\right), \qquad \tau_{coll} = \frac{1}{\bar{\rho}\tilde{\Omega}\sqrt{\frac{2}{3}\tilde{k}}}, \qquad \tilde{\Omega}^*_{coll} = \frac{\tilde{Y}\tilde{k}}{3\sigma_l} \tag{16}$$

with

$$D^*_{32} = D_{32}\frac{1 + \frac{We^N_{coll}}{6}}{1 + \frac{We_{coll}}{6}}, \qquad We_{coll} = \frac{4\tilde{Y}\tilde{k}}{\sigma_l\tilde{\Omega}}, \qquad We^N_{coll} = 12, \qquad D_{32} = \frac{6\tilde{Y}}{\rho_l\tilde{\Omega}}. \tag{17}$$

Finally, the effects of secondary breakup are represented by the source term S_{2ndBU} — this term is modelled based on the work by Pilch and Erdman.[16] The characteristic time scale, τ_{2ndBU}, depends on the secondary breakup mechanism which is related to the magnitude of the droplet Weber number. The model formulation in this case is given by

$$S_{2ndBU} = \alpha_4 Max\left[\frac{\bar{\rho}\tilde{\Omega}}{\tau_{2ndBU}}\left(1 - \frac{\tilde{\Omega}}{\tilde{\Omega^*_{2ndBU}}}\right), 0\right], \qquad \tau_{2ndBU} = T(We_{2ndBU})\frac{D_{32}}{\Delta v_{rel}}\sqrt{\frac{\rho_l}{\rho_g}}, \tag{18}$$

with

$$We^*_{2ndBU} = \frac{6\rho_g\Delta v^2_{rel}\tilde{Y}}{\rho_l\sigma_l\tilde{\Omega}} = \frac{\bar{Y}\tilde{k}}{\sigma_l\tilde{\Omega}^*_{2ndBU}}, \qquad We^*_{2ndBU} = 12(1 + 1.077Oh^{1.6}), \qquad Oh = \frac{\mu_l}{\sqrt{\rho_l\sigma D_{32}}}, \tag{19}$$

and

$$T = \begin{cases} 6(We_{2ndBU} - 12)^{-0.25} & 12 \le We_{2ndBU} \le 18, \\ 2.45(We_{2ndBU} - 12)^{0.25} & 18 \le We_{2ndBU} \le 45, \\ 14.1(We_{2ndBU} - 12)^{0.25} & 45 \le We_{2ndBU} \le 351, \\ 0.766(We_{2ndBU} - 12)^{0.25} & 351 \le We_{2ndBU} \le 2670, \\ 5.5 & We_{2ndBU} \ge 2670. \end{cases} \tag{20}$$

II.B. Modelling of Transition from Dense to Disperse Spray Descriptions

In the combined ELSA model, it is assumed that there exists a spray region where both Eulerian and Lagrangian models are valid. As can be observed in Equation (12), the Eulerian model is able to describe the disperse spray region by accounting for the effects of droplet collision, coalescence and secondary breakup. However, the modelling of the liquid dispersion in the Eulerian model is accomplished with a gradient-based closure, which is not necessarily valid in the disperse region of the spray. In particular, the gradient-based closure is known to be inaccurate when the slip velocity is large.[11,17] Consequently, it can be advantageous to switch to a Lagrangian treatment for the disperse region of the spray, which is the approach is considered here.

II.B.1. Transition Criteria from Dense to Disperse Region

First, the transition region is identified using the ratio between the mean free path between droplets to the SMD, which corresponds to the liquid volume fraction, $\bar{Y}_{disperse}$. Transition cells within the computational grid are then marked using an indicator function, $\beta(\bar{Y})$, which takes on a value of one when all transition criteria are met and otherwise takes on a value of zero. In each marked cell, computational parcels which are representative of a collection of real particles with identical properties (e.g. size, velocity, etc.) are introduced at the beginning of every time step. The transition criteria adopted here are defined as follows:

$$(1)\bar{Y}(x_i, t) < \bar{Y}_{disperse}, \tag{21}$$

$$(2)\bar{Y}_{neighbour}(x_{i,neighbour}, t) > \bar{Y}_{disperse}, \tag{22}$$

$$(3) f_{crit} \cdot m_{ref} < m_{liq}(x_i, t)\,, \tag{23}$$

$$(4) |\nabla \tilde{Y}(x_i, t)| < |\nabla \tilde{Y}_{crit}|\,. \tag{24}$$

The first criteria determines whether or not the local spray structure is sufficiently disperse while the second ensures that the cell lies on the border between the dense and disperse regions. The third criteria controls the computational cost by limiting the creation of computational parcels below a certain mass threshold. The final criteria prevents the creation of computational parcels immediately near the nozzle exit.

To ease the transition between the Eulerian and Lagrangian spray models, source terms are introduced to account for the transfer of conserved quantities from the Eulerian to the Lagrangian model. The rate at which the conserved quantities are transferred is described using a relaxation-time model, defined by a characteristic time, τ. The resulting modified model equations are given by

$$\frac{\partial}{\partial t}\left(\bar{\rho}\right) + \frac{\partial}{\partial x_i}\left(\bar{\rho}\tilde{u}_i\right) = -\frac{\bar{\rho}\tilde{Y}}{\tau}\beta(\tilde{Y})\,, \tag{25}$$

$$\frac{\partial}{\partial t}\left(\bar{\rho}\tilde{u}\right) + \frac{\partial}{\partial x_i}\left(\bar{\rho}\tilde{u}_i\tilde{u}_j\right) = -\frac{\partial}{\partial x_i}\left(\bar{P}\right) - \frac{\partial}{\partial x_i}\left(\lambda_{ij}\right) - \frac{\bar{\rho}\tilde{Y}}{\tau}\tilde{u}_{l,i}\beta(\tilde{Y})\,, \tag{26}$$

$$\frac{\partial}{\partial t}\left(\bar{\rho}\tilde{Y}\right) + \frac{\partial}{\partial x_i}\left(\bar{\rho}\tilde{u}_i\tilde{Y}\right) = -\frac{\partial}{\partial x_i}\left(\widetilde{\bar{\rho}u_i''Y''}\right) - \frac{\bar{\rho}\tilde{Y}}{\tau}\beta(\tilde{Y})\,, \tag{27}$$

$$\frac{\partial}{\partial t}\left(\bar{\rho}\tilde{\Omega}\right) + \frac{\partial}{\partial x_i}\left(\bar{\rho}\tilde{u}_i\tilde{\Omega}\right) = \frac{\partial}{\partial x_i}\left[\left(\frac{\mu_t}{Sc_t}\right)\frac{\partial\tilde{\Omega}}{\partial x_i}\right] + \Psi(S_{init} + S_{turb}) + (1-\Psi)(S_{coll} + S_{2ndBU}) - \frac{\bar{\rho}\tilde{\Omega}}{\tau}\beta(\tilde{Y})\,. \tag{28}$$

II.B.2. Empirical Droplet Size Probability Density Functions

For the modelling of liquid sprays, there exists a number of empirical continutous size PDFs which are used to estimate the underlying droplet distribution, including: the Rosin-Rammler, log-normal and Nukiyama-Tanasawa (NT) models.[6,18–20] At present, droplet sizes are assumed to take the form of the Rosin-Rammler distribution, which is defined as

$$f_D(t, x_i, D) = \frac{qD^{q-1}}{X}\exp\left[-\left(\frac{D}{X}\right)^q\right], \qquad \langle D^n\rangle = X^n\Gamma\left(\frac{n}{q}+1\right), \tag{29}$$

where X is the characteristic droplet size and q is the dispersion coefficient which is a measure of the distribution width. From the Σ-Y model, D_{32} can be calculated using $D_{32} = 6\tilde{Y}/\rho_l\tilde{\Omega}$ and the parameter q can then be calculated using the ratio of D_{32} to D_{10}.[19] Unfortunately, D_{10} cannot be directly calculated from Σ-Y model and at present the ratio between D_{32} and D_{10} is assumed to take a constant value of ≈ 1.75. This corresponds to a specified value of q of approximately ≈ 0.6. More investigation on its validity will be performed in the future.

II.B.3. Assumed Droplet Velocity Distribution Function

The form of the droplet velocity PDF is assumed to be Gaussian. The mean of the distribution is given by the mean liquid mixture velocity which is related to the turbulent liquid flux and is given by

$$\tilde{u}_{l,i} = \tilde{u}_i + \frac{\widetilde{\bar{\rho}u_i''Y''}}{\bar{\rho}\tilde{Y}}\,. \tag{30}$$

The velocity standard deviation, σ_u, is related to the liquid turbulent kinetic energy. The mixture turbulent kinetic energy is given by

$$\tilde{k} = \tilde{Y}\tilde{k_l} + (1-\tilde{Y})\tilde{k_g} + \frac{1}{2}\left(\widetilde{u_i''Y''}\right)^2\left[\frac{1}{\tilde{Y}} + \frac{1}{1-\tilde{Y}}\right]. \tag{31}$$

To obtain the gas turbulent kinetic energy, it is assumed that the turbulent kinetic energy is equally partitioned between liquid and gas phases. Then, the liquid turbulent kinetic energy can be obtained using Equation (31) and used to determine σ_u. The velocity PDF is given by

$$f_{v_i}(v_i) = \frac{1}{\sigma_u\sqrt{2\pi}} exp\left[\frac{-(v_i - \tilde{u}_{l,i})^2}{2\sigma_u^2}\right]. \tag{32}$$

II.B.4. Joint Velocity/Size Probability Density Function

It is assumed that the droplet size and velocity distributions are statistically independent. The joint PDF can then be obtained by taking the product of the droplet velocity and size distribution functions, given by

$$f_{D,v_i}(D, v_i) = f_D(D) f_{v_i}(v_i). \tag{33}$$

While it is recognized that such an assumption does not apply generally to most sprays, this assumption is only used here in the transition region when switching from Eulerian to Lagrangian methods. It is therefore felt that the use of this assumption is not too limiting here. Alternate, more general approaches which allow for dependencies of velocity on size will be examined in future follow-on studies.

II.C. Disperse Spray Region

At present, a Lagrangian method is used for the modeling of the disperse spray region. In this approach, the spray is modeled using a collection of representative droplets in order to describe the PDF, $f_{D,v_i} = f_{D,v_i}(x_i, v_i, D, t)$, which evolves according to the Williams equation given by

$$\frac{\partial}{\partial t}\left(f_{D,v_i}\right) + \frac{\partial}{\partial D}\left(\dot{D} f_{D,v_i}\right) + \frac{\partial}{\partial x_i}\left(v_i f_{D,v_i}\right) + \frac{\partial}{\partial v_i}\left(a_i f_{D,v_i}\right) = \dot{f}_{coll} + \dot{f}_{2ndBU}\,, \tag{34}$$

where D is the parcel diameter, v_i is the parcel velocity and a_i is the parcel acceleration. The terms on the RHS are source terms which correspond to atomization processes relevant in the disperse region of the spray: collision, coalescence and secondary breakup, respectively. Secondary breakup of the spray droplets can be accounted for by using a range of different models, including the TAB,[21] WAVE,[22] KHRT[23] and SSD[24] models. Herin, as the focus is on non-reactive turbulent sprays, evaporation and heat transfer are not considered.

In the Lagrangian approach, the PDF is approximated by a summation of Dirac masses, given by

$$f_{D,v_i} \approx f^L_{D,v_i} = \sum_{\alpha}^{K} \frac{w_\alpha}{W(t, x_i)} \delta(x_i - x_{i,\alpha}) \delta(v_i - v_{i,\alpha}) \delta(D - D_\alpha)\,, \tag{35}$$

where K is the total number of parcels in the computational domain, w_α is the parcel weight and $x_{i,\alpha}$, $v_{i,\alpha}$ and D_α are the position, velocity and size of the α^{th} parcel. The parcel weight is defined as the number of real particles represented by the α^{th} parcel.

For each injected parcel, the parcel weight and the size and velocity abscissas need to be determined. The size and velocity abscissas are obtained by random sampling over a uniform distribution. The weights are then scaled so that the total probability of the injected parcels sums to one. Finally, the size and velocity abscissas are shifted by δD and δv_i so that the injected parcels reproduce the same mass and mean velocity of the assumed droplet size-velocity distribution. Solution to the Williams equation is then approximated by calculating the trajectories of computational parcels which are described by equations of motion obtained by the integration of Newton's second law. The dynamics of the α^{th} parcel is described by the following equations

$$\frac{dx_{i,\alpha}}{dt} = v_{i,\alpha}\,, \tag{36}$$

$$m_\alpha \frac{dv_{i,\alpha}}{dt} = m_\alpha a_{i,\alpha} + D_\alpha\,. \tag{37}$$

Variations in droplet size and mass due to evaporation and droplet energy due to heat transfer can also be tracked but are not currently considered for the non-reactive sprays of interest here.

III. Numerical Results and Discussion

III.A. Implementation Using ANSYS FLUENT

In this section, the accuracy of the standalone Σ-Y, DPM and ELSA models are considered for predicting the droplet size distribution for two different test cases involving liquid sprays in air. The Σ-Y model has been implemented into ANSYS FLUENT using user-defined functions (UDFs). Modifications to FLUENT's

standard SST k-ω model are introduced using user-defined source terms and the Favre-averaged Navier Stokes (FANS) equations are solved using first order discretization and FLUENT's coupled scheme. In the ELSA model, the solution variables from the Σ-Y model are used to compute the mean liquid velocity and SMD which are used to calculate the assumed droplet size-velocity distributions. The parcel properties are initialized using the droplet size-velocity distributions and the parcel trajectories are solved using FLUENT's DPM solver. The effects of drag, turbulence and secondary breakup are also considered in the disperse spray model. In the present study, the effects of droplet collision and coalescence have not been included but will be considered in future studies.

III.B. Primary Breakup for a Turbulent Liquid Jet

The first test spray case consists of a liquid water jet injected into a quiescent environment containing air and measurements were made at different velocities by Wu *et. al*[25] to obtain the droplet size distribution after primary breakup. The Reynolds and Weber number of the liquid jet are 16 000 and 94, respectively. The numerical test case was implemented as a two dimensional (2D) axisymmetric problem and for the Σ-Y and ELSA cases, the mesh consists of 500 cells in the axial direction ($800d$), 50 cells in the radial direction ($250d$) and ten cells across the orifice diameter as seen in Figure 1. The total number of cells in the mesh is 30 000. However for the DPM case, modification of the mesh to only a single cell across the orifice diameter was necessary to obtain a converged solution. It is suspected that the issue is related to the predicted droplet sizes in the vicinity of the nozzle exit which were of the same order of magnitude as the mesh spacing for the original mesh — this is known to cause problems with the coupling between the liquid and gas phases.

The initial droplet size distribution for the DPM model was obtained using FLUENT's plain orifice atomizer model. At each time step, 100 parcels were injected and staggered in space and time to obtain a smoother statistical representation of the spray — this can be seen in Figure 3(a). The effects of drag, turbulence and secondary breakup on the droplets was included. For the combined ELSA model, the Eulerian Σ-Y model is used to predict the behaviour of the dense spray region. At the start of every time step, a check is performed locally to determine if the spray is disperse. When this is true, computational parcels are introduced at the centroid of the transition cells. In this test case, five parcels were introduced in each transition cell, as seen in Figure 3(b).

The disperse spray predicted by the DPM and ELSA models can be seen in Figure 2. Qualitatively, the spray pattern predicted by the ELSA model in Figure 2(b) appears to agree better with the flow images of Wu *et. al*[25] — the experiments indicate a distinct intact liquid core and a narrow distribution of spatially distributed droplets (as predicted by the ELSA model) whereas the spatial spreading predicted by the DPM model appears to be overpredicted compared with the experiment. In addition, the predicted droplet sizes of the Lagrangian DPM model seem overpredicted compared to experiment.

The accuracy of the numerical models was assessed by comparison with the experimentally obtained droplet size distribution of Wu *et. al*[25] at a plane $50d$ downstream of the nozzle, as seen in Figure 3(c). The numerical results computed from the DPM and ELSA models seem to capture reasonably well the same trends as the experiment, however, the DPM model appears to have a larger spread of droplet sizes.

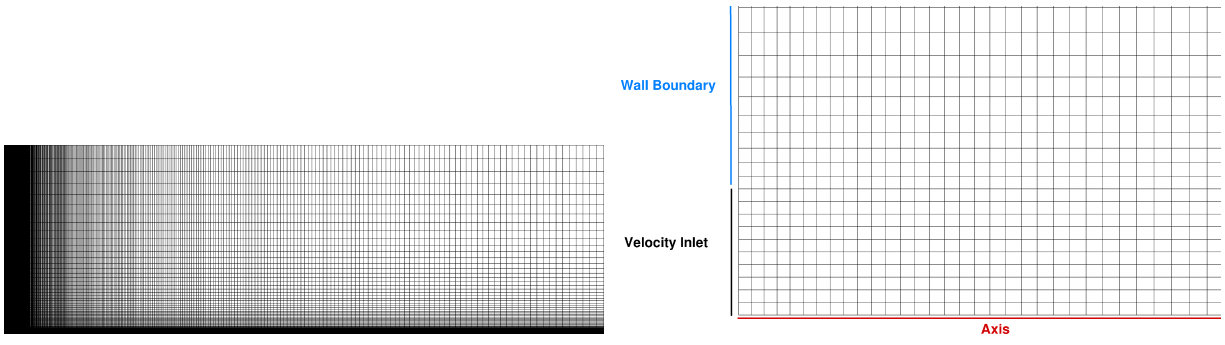

(a) (b)

Figure 1: (a) Mesh for primary breakup of a turbulent liquid jet, (b) Close up of nozzle region.

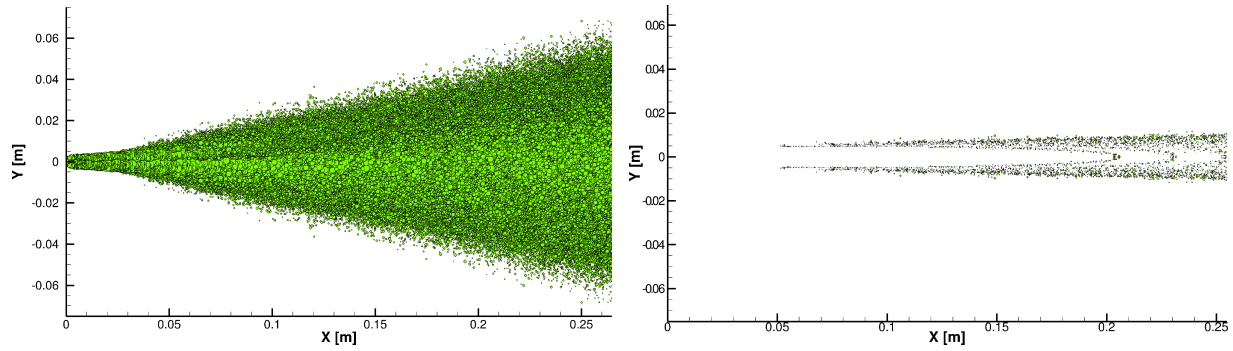

(a) (b)

Figure 2: Droplet sizes predicted by the: (a) DPM model, (b) ELSA model.

III.C. Breakup for a Turbulent Liquid Jet in a Crossflow

The second test case consists of a turbulent liquid water jet in a crossflow of gaseous air, as investigated by Madabhushi *et. al.*[13] A schematic diagram of this spray flowfield is given in Figure 4(a). The Reynolds and Weber number of the liquid jet are $Re_j = 11810$ and $We_j = 24711$, respectively, while the Reynolds and Weber number of the gaseous crossflow are $Re_g = 611200$ and $We_g = 720$, respectively. The computational domain consists of a rectangular box with length of 279 mm, width of 101.6 mm and height of 101.6 mm. The liquid injector is located 114.3 mm from the velocity inlet and has a diameter of 0.762 mm and length of 12.7 mm. For the Σ-Y and ELSA model solutions, the total number of cells is 488 918, depicted in Figure 4(b). Free boundaries are placed at the outlet and the sides of the box are treated as walls. Similar to the previous test case, it was necessary to reduce the resolution of the mesh in the near-nozzle region in order to obtain a converged solution for the Lagrangian DPM model. For the Lagrangian DPM model, the FLUENT plain orifice atomizer model and at each time step, 25 parcels were injected. The parcel injections for the Lagrangian DPM model and ELSA model can be seen in Figure 5(a) and 5(b), respectively.

A qualitative comparison of the jet penetration compared to the experimental correlations of Wu *et. al*[12] and Stenzler *et. al*[26] is shown where the correlations correspond the mean top surface of the liquid jet column. It can be seen that the jet penetrations appear to be underpredicted by the Σ-Y model and over-predicted by the DPM model. For the ELSA model predictions, the droplet spread is wider and the position of droplets seems to better agree with the experimental correlations. Herrmann[6] reported that the correlation of Stenzler *et. al*,[26] which accounts for the crossflow Weber number, shows better agreement with the numerical studies by Herrmann[6] and experiments by Brown *et. al*.[27] Note that measurements for the position of the liquid column were made to up to a maximum of $x/d_{jet} = 10$. For reference, the side and top view of the velocity fields predicted by the Σ-Y, DPM and ELSA models are given in Figures 6(a)-6(c), and Figures 7(a)-7(c), respectively. In the predictions by the Σ-Y (Figure 6(a) and 7(a)) and ELSA (Figure 6(c) and 7(c)) models, a low momentum region can be identified immediately downstream of the jet — this occurs because of the significant momentum exchange from the airstream to the liquid column, which causes deformation of the liquid column in the leeward direction. In addition, from the top views, a wake region can be identified downstream of the liquidt jet. The low momentum region is absent in Figure 6(b) and 7(b) because the DPM model does not explicitly model the liquid column and this is a known issue with the model as volume effects of the liquid core are not incoroprated in this disperse phase treatment.[13]

The accuracy of the predicted droplet velocity and size was compared against the experimental results obtained by Madabhushi *et. al*[13] in Figure 9(a) and 9(b), respectively. In the experiment, measurements were made for the droplet velocity and size in the transverse direction of the mid-plane at 25.4 mm downstream of the jet orifice. It can be seen that close to the wall, the droplet velocity predicted by the Σ-Y model agrees well with experiment, until about $x = 0.01m$, at which point the droplet axial velocity is over-predicted. The ELSA model predicts a similar droplet axial velocity to the Σ-Y model in the near wall region and this is likely because the ELSA model has not transitioned to the disperse phase model in this region. In Figure 9(b), the SMD is under-predicted by the Σ-Y model and over-predicted by the DPM model. For the ELSA model, while the SMD is over-predicted in the bottom half region, the results seem reasonable in the top half region. In both figures, it can be argued that the predictions of the ELSA model match the experimental results better than either the Σ-Y or DPM model.

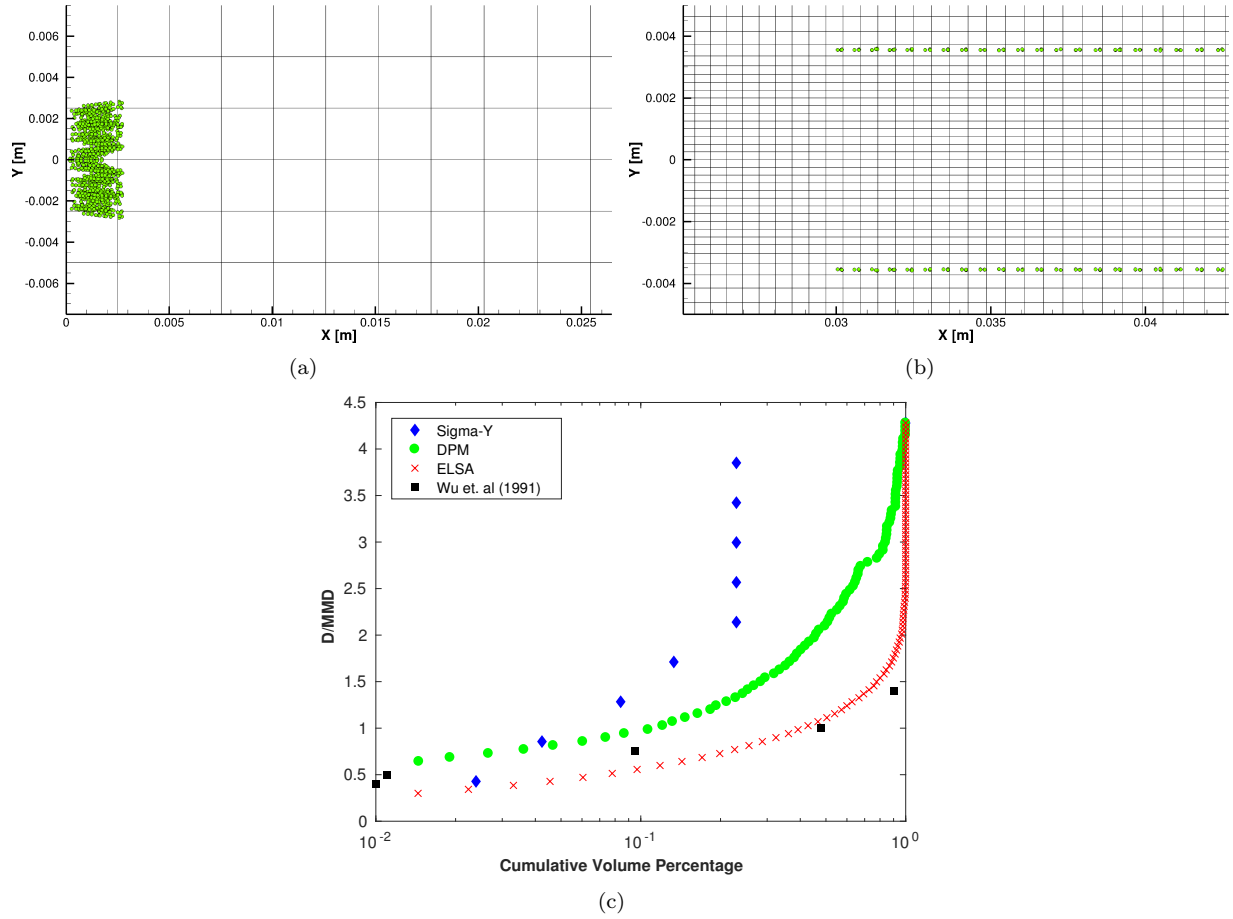

Figure 3: (a) Parcel Injections for the Lagrangian DPM Model, (b) Parcel Injections for the ELSA Model, (c) Comparison between experimental and numerical droplet distributions.

IV. Conclusions

An approach to coupling of Eulerian and Lagrangain methods in the so-called ELSA model has been proposed. The performance of the resulting ELSA model for predicting the droplet size distribution has been assessed by comparing its predictions to those of the Σ-Y and DPM models, as well as to available experimental data for two spray flow cases. In the first test case, the primary breakup of a turbulent liquid jet, the initial results between the ELSA model and experiment appear to agree reasonably well. In the second test case, the breakup of a turbulent liquid jet in a crossflow, it can be seen that the Σ-Y and ELSA models are capable of predicting the low momentum region immediately downstream of the liquid column — the DPM model is unable to detect this region. In both cases, the predictions of the ELSA model are arguably better in agreement with experiment than those of the Σ-Y and DPM models — the ELSA model appears quite promising in its ability to predict the behaviour of turbulent liquid sprays.

Acknowledgments

Computations were primarily performed on the GPC supercomputer at the SciNet HPC Consortium. SciNet is funded by: the Canada Foundation for Innovation under the auspices of Compute Canada; the Government of Ontario; Ontario Research Fund - Research Excellence; and the University of Toronto. Financial support for this project was primarily provided by Pratt & Whitney Canada and NSERC through their Industrial Research Chair in Aviation Gas Turbine Combustion/Emissions Research and Design System Optimization program.

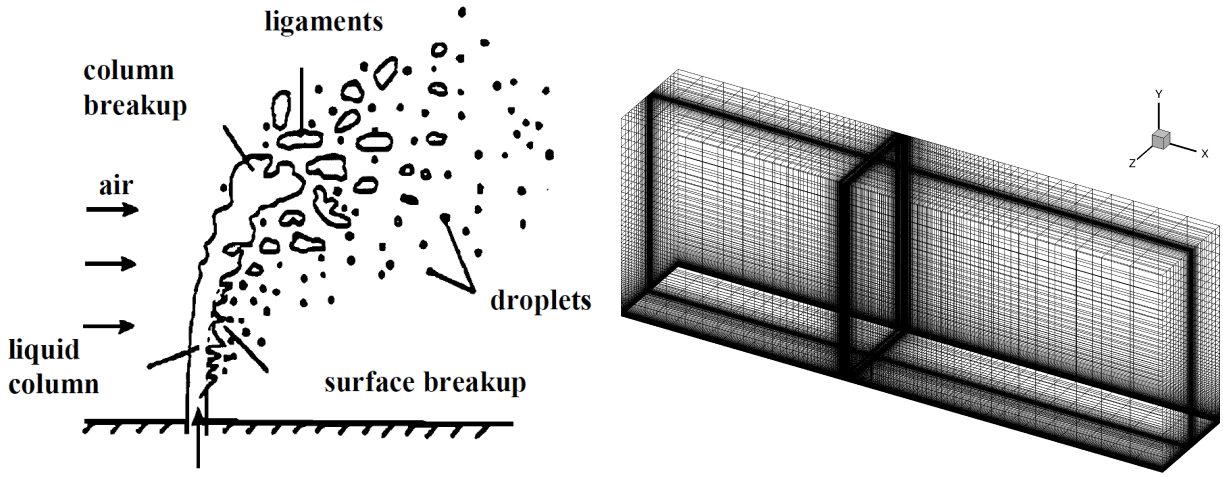

(a) (b)

Figure 4: (a) Schematic diagram of a liquid jet in a crossflow, (b) Mesh for turbulent liquid jet in a crossflow.

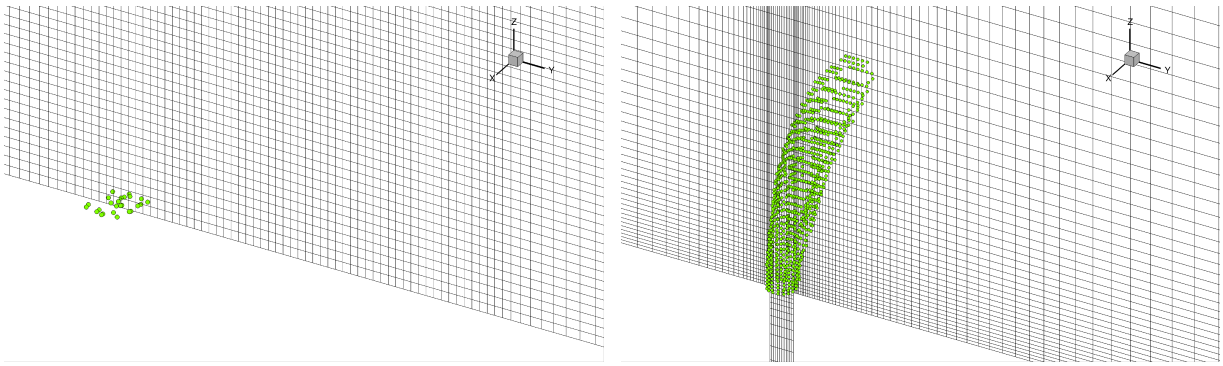

(a) (b)

Figure 5: (a) Schematic diagram of a liquid jet in a crossflow, (b) Mesh for turbulent liquid jet in a crossflow.

References

[1]Faeth, G., Hsiang, L.-P., and Wu, P.-K., "Structure and breakup properties of sprays," *International Journal of Multiphase Flow*, Vol. 21, Supplement, No. 0, 1995, pp. 99–127.

[2]Datta, A. and Som, S. K., "Effects of spray characteristics on combustion performance of a liquid fuel spray in a gas turbine combustor," *International Journal of Energy Research*, Vol. 23, No. 3, 1999.

[3]Jiang, X., Siamas, G., Jagus, K., and Karayiannis, T., "Physical modelling and advanced simulations of gas–liquid two-phase jet flows in atomization and sprays," *Progress in Energy and Combustion Science*, Vol. 36, No. 2, 2010, pp. 131–167.

[4]Fox, R. O., "Large-Eddy-Simulation Tools for Multiphase Flows," *Annual Review of Fluid Mechanics*, Vol. 44, No. 1, 2012, pp. 47–76.

[5]Subramaniam, S., "Lagrangian–Eulerian methods for multiphase flows," *Progress in Energy and Combustion Science*, Vol. 39, No. 2–3, 2013, pp. 215–245.

[6]Herrmann, M., "Detailed Numerical Simulations of the Primary Atomization of a Turbulent Liquid Jet in Crossflow," *Journal of Engineering for Gas Turbines and Power*, Vol. 132, No. 6, 2010, pp. 061506.

[7]Navarro-Martinez, S., "Large eddy simulation of spray atomization with a probability density function method," *International Journal of Multiphase Flow*, Vol. 63, 2014, pp. 11–22.

[8]Vallet, A., Burluka, A. A., and Borghi, R., "Development of an Eulerian Model for the "Atomization" of a Liquid Jet," *Atomization and Sprays*, Vol. 11, No. 6, 2001, pp. 619–642.

[9]Chesnel, J., Reveillon, J., Menard, T., and Demoulin, F.-X., "Large Eddy Simulation of Liquid Jet Atomization," *Atomization and Sprays*, Vol. 21, No. 9, 2011, pp. 711–736.

[10]Marchisio, D. L. and Fox, R. O., *Computational Models for Polydisperse Particulate and Multiphase Systems*, Cambridge University Press, New York, 2013.

[11]Lebas, R., Menard, T., Beau, P., Berlemont, A., and Demoulin, F., "Numerical simulation of primary break-up and atomization: DNS and modelling study," *International Journal of Multiphase Flow*, Vol. 35, No. 3, 2009, pp. 247–260.

[12]Wu, P.-K., Kirkendall, K. A., Fuller, R. P., and Nejad, A. S., "Breakup processes of liquid jets in subsonic crossflows," *Journal of Propulsion and Power*, Vol. 13, No. 1, 1997, pp. 64–73.

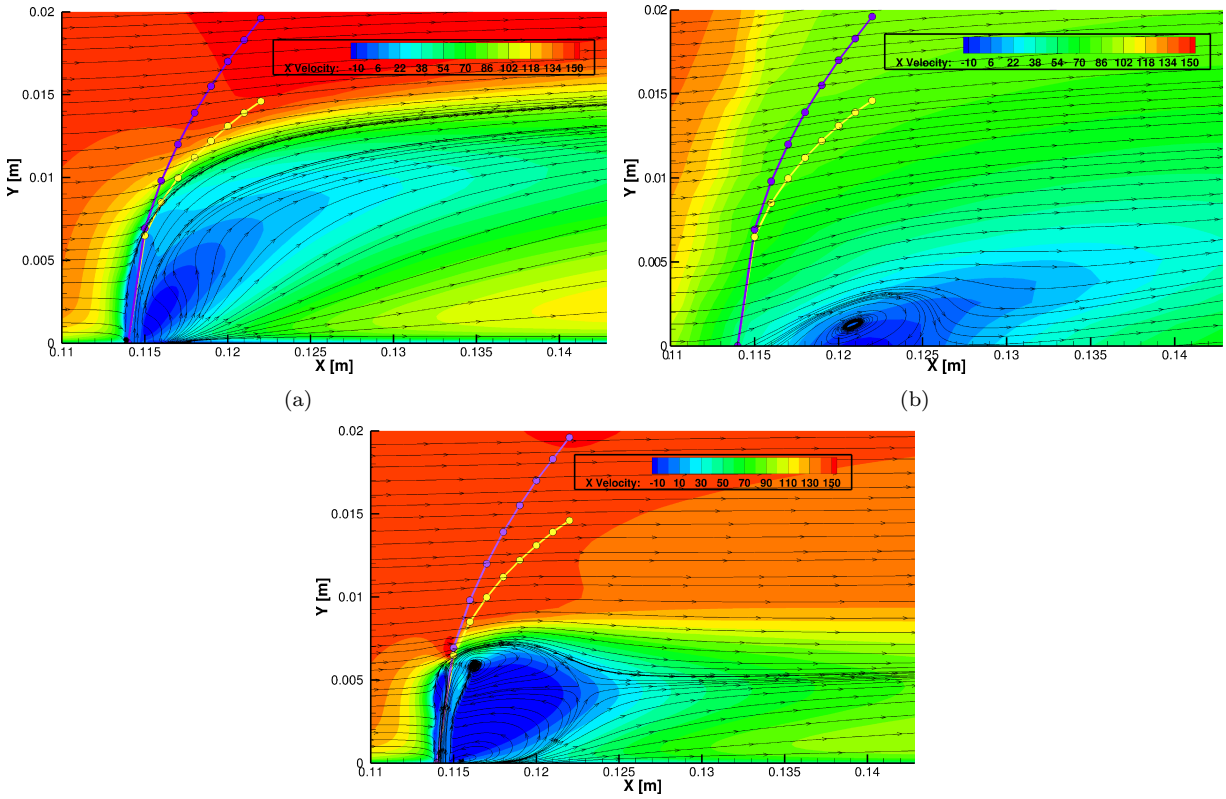

Figure 6: Streamwise velocity contours and streamlines as predicted by the: (a) Σ-Y Model, (b) Lagrangian DPM Model, (c) ELSA Model.

[13]Madabhushi, R. K., Leong, M. Y., and Hautman, D. J., "Simulation of the Break-up of a Liquid Jet in Crossflow at Atmospheric Conditions," *ASME Turbo Expo 2004: Power for Land, Sea, and Air*, American Society of Mechanical Engineers, 2004, pp. 697–704.

[14]Ning, W., Reitz, R. D., Diwakar, R., and Lippert, A. M., "An Eulerian-Lagrangian Spray and Atomization Model with Improved Turbulence Modeling," *Atomization and Sprays*, Vol. 19, No. 8, 2009, pp. 727–739.

[15]Beau, P., Ménard, T., Lebas, R., Berlemont, A., Tanguy, S., and Demoulin, F.-X., "Numerical Jet Atomization: Part II–Modeling Information and Comparison With DNS Results," *ASME 2006 2nd Joint US-European Fluids Engineering Summer Meeting Collocated With the 14th International Conference on Nuclear Engineering*, American Society of Mechanical Engineers, 2006, pp. 555–563.

[16]Pilch, M. and Erdman, C., "Use of breakup time data and velocity history data to predict the maximum size of stable fragments for acceleration-induced breakup of a liquid drop," *International Journal of Multiphase Flow*, Vol. 13, No. 6, 1987, pp. 741–757.

[17]Andreini, A., Bianchini, C., Puggelli, S., and Demoulin, F., "Development of a turbulent liquid flux model for Eulerian–Eulerian multiphase flow simulations," *International Journal of Multiphase Flow*, Vol. 81, 2016, pp. 88–103.

[18]Babinsky, E. and Sojka, P., "Modeling drop size distributions," *Progress in Energy and Combustion Science*, Vol. 28, No. 4, 2002, pp. 303–329.

[19]Yoon, S. S., "Droplet distributions at the liquid core of a turbulent spray," *Physics of Fluids*, Vol. 17, No. 3, 2005, pp. 035103.

[20]Majhool, A. A. A.-K. and Watkins, A., "Spray algorithm without interface construction," *Journal of Computational Physics*, Vol. 231, No. 9, 2012, pp. 3647 – 3662.

[21]O'Rourke, P. and Amsden, A., "The TAB Method for Numerical Calculation of Spray Droplet Breakup," *SAE Technical Paper 872089*, 1987.

[22]Reitz, R., "Modeling atomization processes in high-pressure vaporizing sprays," *Atomisation and Spray Technology*, Vol. 3, No. 4, 1987, pp. 309–337.

[23]Beale, J. C., Reitz, R. D., et al., "Modeling spray atomization with the Kelvin-Helmholtz/Rayleigh-Taylor hybrid model," *Atomization and sprays*, Vol. 9, No. 6, 1999, pp. 623–650.

[24]Apte, S., Gorokhovski, M., and Moin, P., "{LES} of atomizing spray with stochastic modeling of secondary breakup," *International Journal of Multiphase Flow*, Vol. 29, No. 9, 2003, pp. 1503–1522.

[25]Wu, P.-K., Ruff, G. A., and Faeth, G. M., "Primary Breakup in Liquid/Gas Mixing Layers," *29th Aerospace Sciences Meeting, Aerospace Sciences Meetings*, American Institute of Aeronautics and Astronautics, 1990.

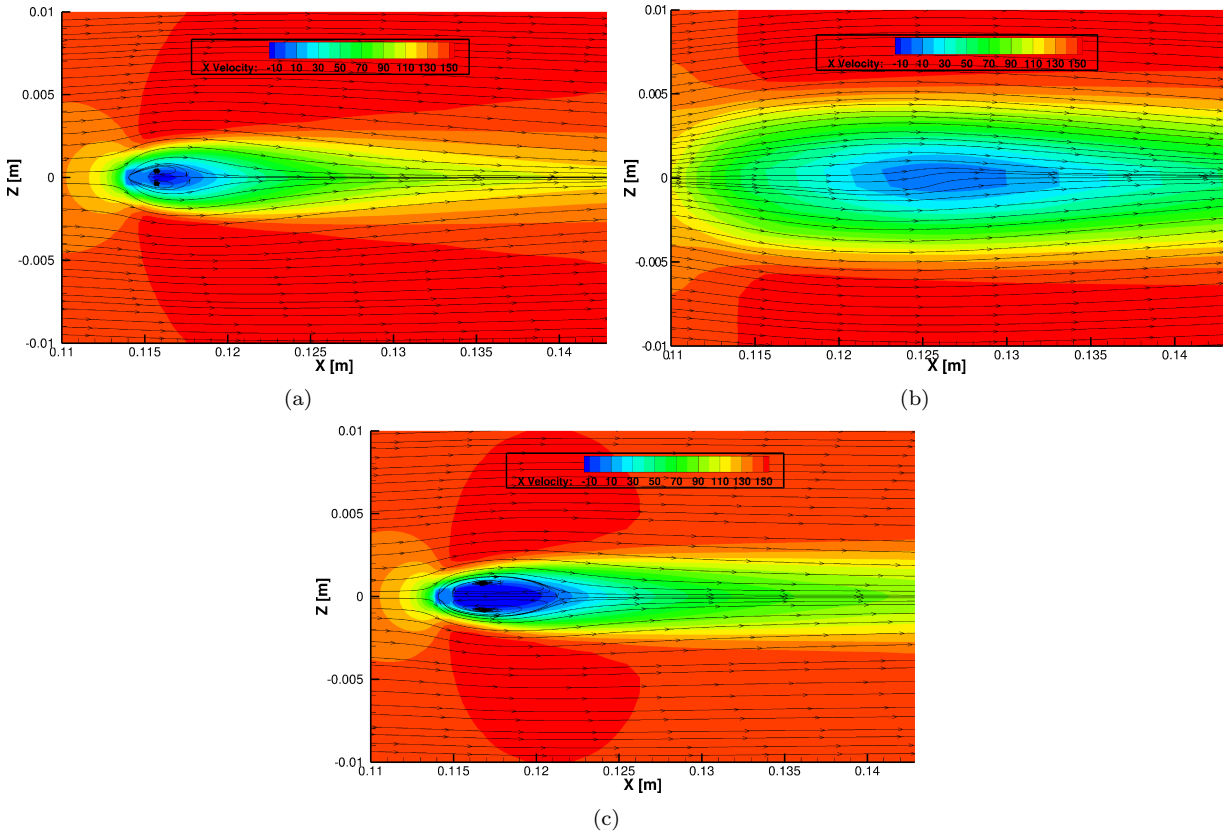

Figure 7: Streamwise velocity contours and streamlines as predicted by the: (a) Σ-Y Model, (b) Lagrangian DPM Model, (c) ELSA Model.

[26]Stenzler, J. N., Lee, J. G., Santavicca, D. A., and Lee, W., "Penetration of Liquid Jets in a Cross-Flow," *Atomization and Sprays*, Vol. 16, No. 8, 2006, pp. 887–906.

[27]Brown, C. T. and McDonell, V. G., "Near field behavior of a liquid jet in a crossflow," *ILASS Americas 19th Annual Conference on Liquid Atomization and Spray Systems*, 2006.

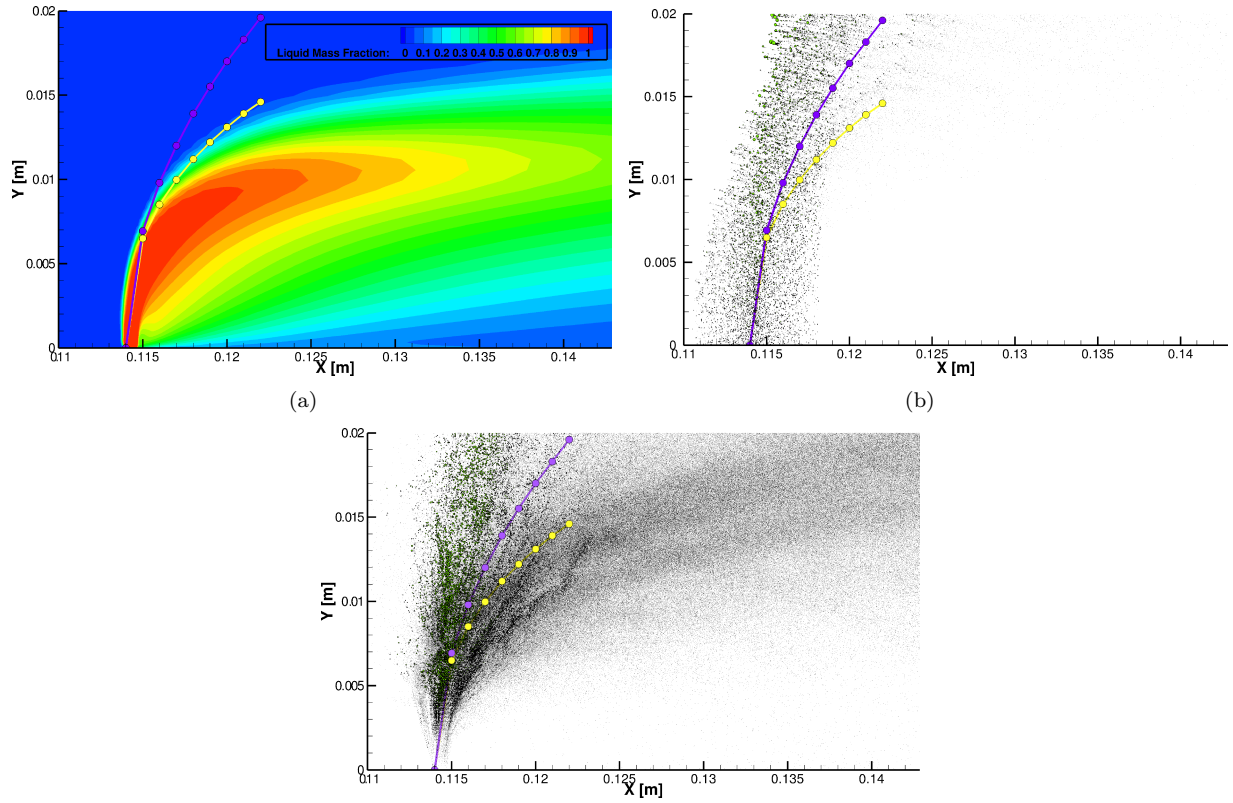

Figure 8: Jet penetration compared to correlations from Wu *et. al*[25] (upper curve) and Stenzler *et. al*[26] (lower curve) for the: (a) Σ-Y Model, (b) Lagrangian DPM Model, (c) ELSA Model.

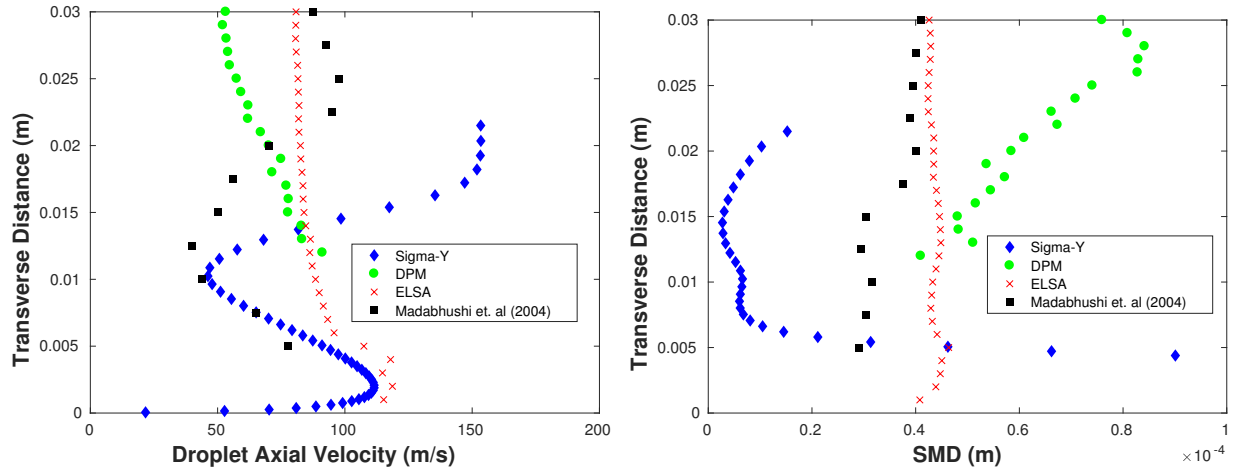

Figure 9: Transverse profile at $x = 33.3d$ downstream of the orifice in the mid-plane ($z = 0$), comparing the droplet: (a) velocity, (b) SMD.